Discover Applied Sciences

RESEARCH Open Access

Magnetically tunable surface phonon polaritons in ZnO and ZnO:Mn ceramics

O. Melnichuk[1], N. Korsunska[2], L. Melnichuk[1] and L. Khomenkova[2,3*]

*Correspondence:
L. Khomenkova
khomen@ukr.net
[1]Nizhyn Mykola Gogol State University, 2 Hrafska Str., Nizhyn 16600, Ukraine
[2]V. Lashkaryov Institute of Semiconductor Physics at the National Academy of Sciences of Ukraine, 41 Prospekt Nauky, Kyiv 03028, Ukraine
[3]National University "Kyiv Mohyla Academy", 2 Skovorody Str., Kyiv 04070, Ukraine

Abstract
The excitation conditions and spectra signatures of surface phonon polaritons and plasmon–phonon polaritons in ZnO and Mn-doped ZnO ceramics have been theoretically analyzed and experimentally probed. Specular infrared reflection and attenuated total reflection spectroscopy were employed to investigate their dispersion relations. A single-oscillator model was used to describe the dielectric permittivity of ZnO ceramics, accounting for additive phonon and plasmon contributions. Theoretical and experimental dispersion curves were examined in the 100–4000 cm^{-1} and 240–4000 cm^{-1} spectral range, respectively. Additionally, the effect of an external magnetic field on surface polaritons was explored, revealing magnetically tunable optical responses. These findings contribute to the development of ZnO-based plasmonic and photonic devices, particularly in infrared and terahertz applications.

Keywords Surface polaritons, Attenuated total reflection, Dielectric permittivity, Ceramics, Zinc oxide, Dispersion relations

1 Introduction

The increasing applications of surface waves in modern photonic and optoelectronic devices have driven significant interest in the study of electromagnetic waves in crystals [1–6]. In particular, surface polaritons—phonon, plasmon, and plasmon–phonon polaritons—have been extensively explored in optically isotropic and anisotropic materials due to their relevance in sensing, energy transfer, and subwavelength optical components [7–12]. While substantial progress has been made in understanding these excitations, their behavior in non-metallic films and ceramics as well as under external perturbations, such as magnetic fields, remains less studied [4, 6, 11, 12].

Surface polaritons are hybrid electromagnetic waves that arise from strong coupling between photons and collective excitations in a material [4, 13, 14]. Their properties are highly sensitive to material composition, electronic structure, and external stimuli. In particular, the application of a magnetic field can modify surface polariton dispersion and introduce nonreciprocal propagation effects, offering new functionalities in magneto-optical devices [15, 16].

Theoretical studies have predicted that surface polaritons can be excited in polar semiconductors and can be sensitive to an external magnetic field [2, 9, 13, 14]. Similar findings were experimentally confirmed in InSb single crystals, where the excitation of surface magnetoplasmon-phonon polaritons was observed as a function of magnetic field strength [11, 12]. Despite these advancements, the effect of magnetic fields on surface polaritons in non-magnetic oxides remains an open question.

Some research groups have shown that magnetic fields influence not only the properties of magnetic semiconductors but also induce various magneto-optical effects in nominally non-magnetic materials [14–20]. Theoretical models suggest that the increase of the magnetic field strength can alter the optical phonon interactions and, consequently, the surface phonon polariton dispersion [21]. Besides, in the infrared reflection spectra of non-magnetic materials, sharp peaks near the transverse optical phonon frequency can be observed being dependent on the strength of applied magnetic fields [20–22].

Among non-magnetic polar semiconductors, ZnO is a fascinating material in this context. It combines a wide bandgap, high optical transparency, and tunable electrical conductivity, making it a promising candidate for plasmonic and photonic applications. Theoretical investigations have explored the influence of free carrier concentration and magnetic fields on the infrared reflection spectra of ZnO single crystals [13, 14, 22, 23]. However, these studies lack experimental validation. Furthermore, magneto-optical phenomena were much less addressed for ZnO-based ceramics, especially, for those doped with magnetic dopants.

This study aims to address the gap in understanding surface phonon and plasmon–phonon polaritons in ZnO-based ceramics under magnetic fields. We focus on the spectral signatures and magnetically induced dispersion of these polaritons in undoped and Mn-doped ZnO ceramics. Specular infrared reflection and attenuated total reflection spectroscopy were employed to probe these polaritonic features, providing information about their frequency-dependent behavior under applied magnetic fields. While these experiments do not directly track surface wave propagation, the results offer insights into the magneto-optical response and tunability of ZnO-based functional materials, contributing to potential plasmonic and photonic applications in the infrared and terahertz ranges.

2 Experimental details

ZnO-based ceramics were prepared using a high-purity commercial ZnO powder (99.99%). The powder was dispersed in distilled water and mixed using a magnetic stirrer to break up large agglomerates and to improve the homogeneity of the powder prior to compaction. To prepare Mn-doped ZnO samples, an aqueous solution of $MnSO_4$ was added directly to the ZnO suspension in amounts corresponding to target manganese concentrations of $N_{Mn} = 10^{20}$ and 10^{21} cm^{-3}. The suspensions were then dried at 150 °C during 8 h to remove residual moisture and stored at room temperature prior to compaction. Both undoped and Mn-doped ZnO powders were uniaxially pressed into rectangular pellets under a pressure of 50 MPa for 30 min. The compacted samples were placed in a muffle furnace, heated to 1100 °C, annealed in air at this temperature for 3 h, and then cooled to room temperature inside the furnace.

The attenuated total reflection (ATR) spectra were measured using a Shimadzu IRTracer-100 spectrophotometer equipped with a QATR-10 accessory, allowing for

measurements in the spectral range of 240–4000 cm^{-1} at a fixed angle of incidence of IR radiation ($\phi = 45°$) on an ATR "semi-cylinder" made of diamond ($\varepsilon = 6.08$). The specular infrared reflection (IRR) spectra were recorded in the same spectral range with a SRM-8000A specular reflectance tool. The incidence angle of the excitation IR light on sample surface was ~10°. Spectral dependencies of the reflection coefficient were obtained by averaging the maximum number of scans (240 scans) performed at each point in the spectrum. The reflection coefficient was determined with an accuracy of 1%. The resolution in the specified range was 0.1 cm^{-1}. As a reference sample, a single 6H-SiC crystal with a carrier concentration $n_0 = 10^{16}$ cm^{-3} and known reflection coefficient over 240–4000 cm^{-1} spectral range was used. The accuracy of determining the IR reflection minima was ± 0.1 cm^{-1}, the uncertainty in the reflection coefficient did not exceed 1%, and the dielectric constant was determined with an accuracy of ± 0.01.

The orientation of the ceramic samples and the magnetic field was chosen as $c||y$, $\vec{k} \perp c, xy \parallel c$, $\vec{H} \perp \vec{k}$, $\vec{H}||y$, $k_x = k, k_{y,z} = 0$. The schematic presentation is shown in Fig. 1. Magnetic field with the strength $H = 3$ kOe and 10 kOe was obtained from permanent Nd magnets.

The experimental setup and the sample placement between the poles of the magnets on a special holder is shown in Fig. 2a. The magnetic field was oriented parallel to the surface of the ceramic (Fig. 2b). All measurements were carried out at room temperature.

3 Results and discussion

3.1 Specular IRR spectra of ZnO-based ceramics

The excitation and propagation of surface polaritons along the surface of ZnO and ZnO:Mn ceramics are considered for the configuration shown in Fig. 1, where the *x*-axis corresponds to the direction of the electromagnetic wave propagation, and the *c*-axis of ZnO grains is aligned along the *y*-axis. As shown by XRD study of similar ceramics in

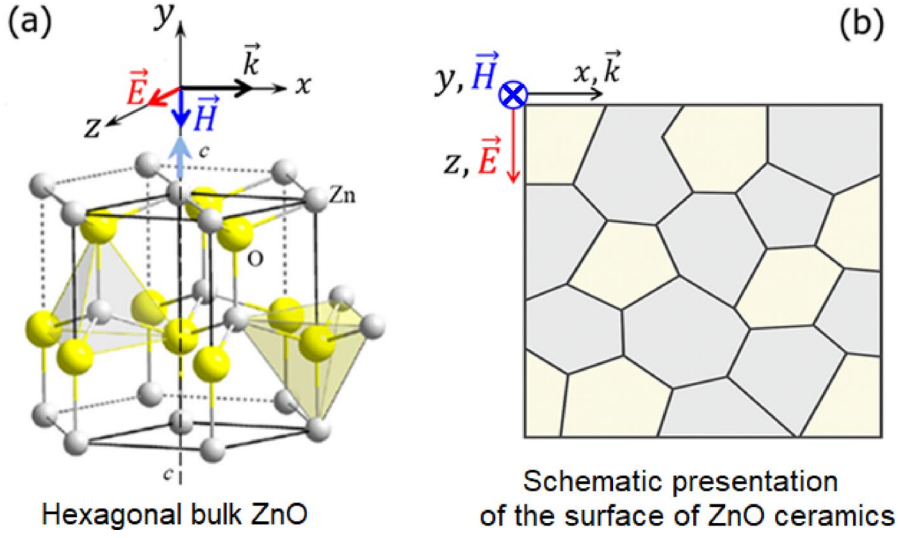

Fig. 1 Schematic presentation of the orientation of the direction of electromagnetic wave propagation (vectors $\vec{E}$, $\vec{H}$ and wave vector $\vec{k}$), and the coordinate axes (*x*, *y*, *z*) in hexagonal bulk ZnO (**a**) and along the surface of polycrystalline ZnO ceramics (**b**) for the study of surface polaritons. The light blue arrow in **a** indicates the direction of the crystallographic *c*-axis in the ZnO lattice. The differently colored grains in **b** represent crystallites whose crystallographic *c*-axes are not perfectly aligned with the *y*-axis but are randomly distributed within a cone of orientations, illustrating the polycrystalline nature of the ceramics

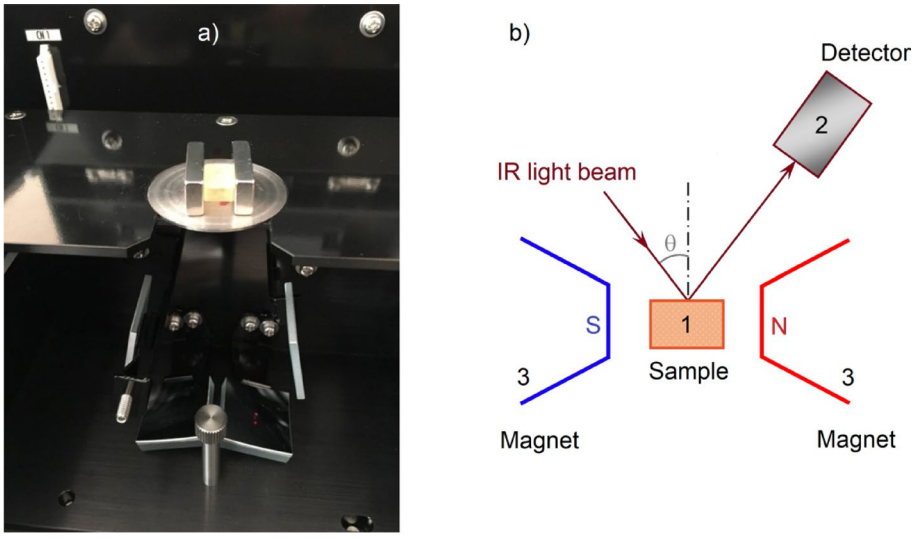

Fig. 2 **a** SRM-8000A accessory for measuring specular IRR spectra of ZnO ceramics in a magnetic field; **b** schematic of the experimental setup: 1—sample; 2—IR detector of the Shimadzu IRTracer-100 spectrometer; 3—poles of the magnets

[24, 25], the orientation of ZnO grains is random and the shape of the infrared reflection spectra closely matches that expected for the $\vec{E}\perp c$ polarization. As previously demonstrated in [25], the contribution from $\vec{E}||c$ polarization is negligible in these ceramics and becomes noticeable only in the narrow range of 380–400 cm^{-1}, where a slight deviation between experimental and simulated spectra for $\vec{E}\perp c$ is observed. This behavior arises from the fact that in randomly oriented polycrystalline materials, the $\vec{E}\perp c$ component dominates the infrared reflection response whereas the $\vec{E}||c$ contribution emerges only when A_1 mode is excited along the *c*-axis [25]. It was also reported that the IRR spectrum remains nearly unchanged when the angle between the electric field vector and the *c*-axis is within 5°, which justifies the use of $\vec{E}\perp c$ polarization alone for spectra modelling. Based, on these findings, electromagnetic wave propagation along the surface of polycrystalline ZnO ceramics can be considered using approach developed for ZnO single crystals [21, 23] and adopted later for polycrystalline ZnO thin films [9, 23] and undoped ZnO ceramics [24, 25]. Thus, reflection coefficient *R*(ν) in infrared spectral range, i.e. specular IRR and ATR spectra for ZnO ceramics are simulated, according to the approaches described in [13, 21, 23], for conditions $c||y$, $\vec{k}\perp c, xy \parallel c$, $\vec{H}\perp\vec{k}$, $\vec{H}||y$. Hereafter, all results and their discussion will be presented for such conditions unless otherwise specified.

For ZnO and ZnO:Mn ceramics, the dielectric permittivity is a tensor determined accordingly [3, 17] as:

$$\varepsilon = \begin{pmatrix} \varepsilon_1 & i\varepsilon_2 & 0 \\ -i\varepsilon_2 & \varepsilon_1 & 0 \\ 0 & 0 & \varepsilon_3 \end{pmatrix}, \quad (1)$$

where ε_1, ε_2 and ε_3 are matrix elements:

$$\begin{aligned}
\varepsilon_1 &= \varepsilon_\infty \left(1 + \frac{\nu_L^2 - \nu_T^2}{\nu_T^2 - \nu^2 - i\gamma_f \nu} + \frac{\nu_p^2 (\nu + i\gamma_p)}{\nu \left(\Omega^2 - (\nu + i\gamma_p)^2\right)}\right), \\
\varepsilon_2 &= \frac{\varepsilon_\infty \nu_p^2 \Omega}{\nu \left((\nu + i\gamma_p)^2 - \Omega^2\right)}, \\
\varepsilon_3 &= \varepsilon_\infty \left(1 + \frac{\nu_L^2 - \nu_T^2}{\nu_T^2 - \nu^2 - i\gamma_f \nu} - \frac{\nu_p^2}{\nu (\nu + i\gamma_p)}\right),
\end{aligned} \tag{2}$$

ε_∞—the high-frequency dielectric permittivity; ν_L, ν_T—the frequencies of the longitudinal and transverse optical phonons, respectively; ν_p—the plasma resonance frequency; γ_p—the plasmon damping coefficient; γ_f—the phonon damping coefficient; $\Omega = eH/m^* c_0$—the cyclotron frequency, m^*—effective electron mass ($m^* = 0.26 m_e$), c_0—the light speed, H—magnetic field strength. The electron effective mass is considered as a tensor also. More details can be seen in Supplement information and Refs. [17, 23]. The reflection coefficient $R(\nu)$ can be estimated from well-known relation $R(\nu) = [(\sqrt{\varepsilon} - 1)/(\sqrt{\varepsilon} + 1)]^2$ (see Supplement information). Besides, the free carrier concentration can be calculated using relation $\omega_p = \sqrt{4\pi n_0 e^2 / m^* \varepsilon_\infty}$ from known plasmon frequency ($\omega_p = 2\pi\nu_p$) [9, 13].

Figure 3a presents the theoretical dependence $R(\nu)$ for specular infrared reflection for ZnO ceramics with different free carrier concentration varying in the range $n_0 = 1.5{\cdot}10^{15} \div 1.2{\cdot}10^{18}$ cm^{-3} without application of magnetic field. For the simulation, the self-consistent parameters for the case (Fig. 1) were taken as $\varepsilon_\infty = 3.95$, $\varepsilon_0 = 8.1$, $\nu_T = 412$ cm^{-1}, $\nu_L = 585$ cm^{-1} [24]. The variation of free carrier concentration ($n_0 = 1.15{\cdot}10^{15}$ cm^{-3} (1), $7.2{\cdot}10^{17}$ cm^{-3} (2), $2.9{\cdot}10^{18}$ cm^{-3} (3), $6.4{\cdot}10^{18}$ cm^{-3} (4), and $1.15{\cdot}10^{19}$ cm^{-3} (5)) was considered via the variation of plasmon frequency and its damping coefficient: $\nu_{p\perp} = \gamma_{p\perp} = 1$ cm^{-1} (curve 1), 250 cm^{-1} (curve 2), 500 cm^{-1} (curve 3), 750 cm^{-1} (curve 4), and 1000 cm^{-1} (curve 5) as well as. The phonon damping coefficient is $\gamma_{f\perp} = 11$ cm^{-1} for all curves.

The inset in Fig. 3 shows the real $\varepsilon'(\nu)$ and imaginary $\varepsilon''(\nu)$ parts of dielectric permittivity for undoped ZnO ceramics obtained by solving the inverse problem of specular IRR spectroscopy [17]. This procedure involves extracting $\varepsilon'(\nu)$ and $\varepsilon''(\nu)$ from the measured reflectance R(ν) by fitting the data to the Fresnel equations for the sample surface. The resulting dependences are similar to those reported for ZnO single crystals [13, 17]. The estimated carrier concentration is $n_0 = 7.2{\cdot}10^{17}$ cm^{-3}, $\nu_p = 100$ cm^{-1}, $\gamma_p = 100$ cm^{-1} i $\gamma_f = 15$ cm^{-1}. The analysis of the $\varepsilon'(\nu)$ revealed the existence of the frequency range where $\varepsilon'(\nu) \le -1$. This indicates the anomalous dispersion region of ZnO ceramics and the possibility to excited surface phonon polaritons at the ceramic surface—air interface. The frequency "window" is 412–559 cm^{-1} as marked by a yellow color (Fig. 3a, inset).

The shape of experimental specular IRR spectra for ZnO and ZnO:Mn ceramics was found to be similar while a slight increase of reflection coefficient $R(\nu)$ in the Reststrahlen band was observed for ZnO:Mn ceramics.

The similar $R(\nu)$ rise was discovered for the samples subjected to magnetic field as shown by Fig. 3b for ZnO:Mn ceramics with $n_{Mn} = 10^{21}$ cm^{-3}. The fitting of experimental data is shown by solid lines. It is seen that good agreement of the simulation of data presented by symbols 1 (without magnetic field) can be obtained with $\varepsilon_\infty = 3.95$, $\varepsilon_0 = 8.1$, $\nu_T = 412$ cm^{-1}, $\nu_L = 591$ cm^{-1}, $\nu_p = 350$ cm^{-1}, $\gamma_p = 700$ cm^{-1} and $\gamma_f = 38$ cm^{-1}. For

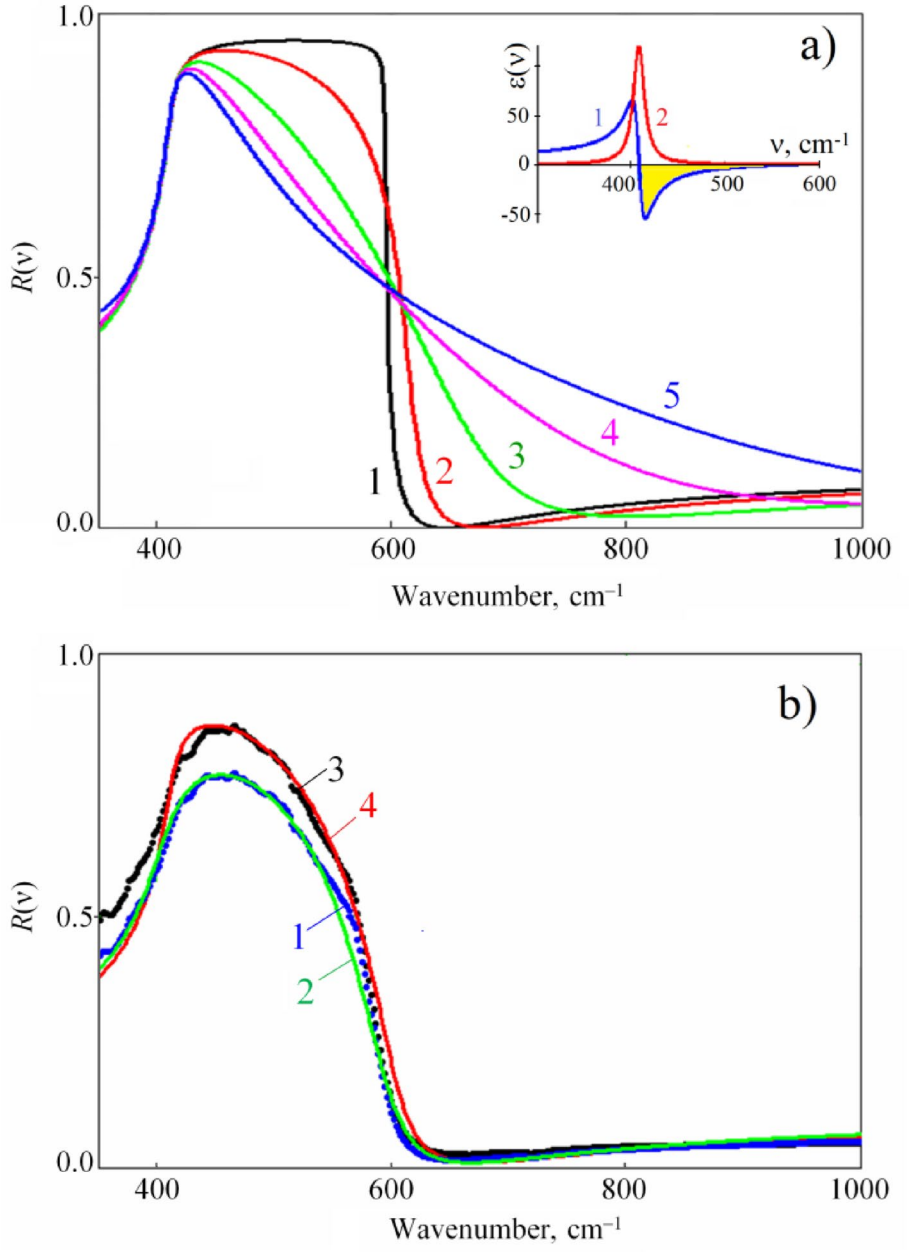

Fig. 3 **a** Theoretical specular IRR spectra of the ZnO ceramics with different free carrier concentrations: The inset shows the frequency dependence of real part ε′(ν) (curve 1) and imaginary part ε′′(ν) (curve 2) of ZnO dielectric permittivity and the frequency range where surface phonon polaritons can appear. **b** Experimental specular IRR spectra (symbols 1, 3) and their simulation (curves 2, 4) of the ZnO:Mn ceramics with Mn content $n_{Mn} = 10^{21}$ cm^{-3}, without (1,2) and with magnetic field $H = 10$ κOe (3,4). The estimated carrier concertation for ZnO:Mn ceramics is $n_0 = 1.4 \cdot 10^{18}$ cm^{-3}

the case of applied magnetic field (data presented by symbols 3), the best fitting occurs when $\varepsilon_\infty = 3.8$, $\varepsilon_0 = 8.1$, $\nu_T = 412$ cm^{-1}, $\nu_L = 591$ cm^{-1}, $\nu_p = 350$ cm^{-1}, $\gamma_p = 1200$ cm^{-1} and $\gamma_f = 15$ cm^{-1}. The free carrier concentration was estimated to be nearly the same ($n_0 = 1{,}4 \cdot 10^{18}$ cm^{-3}) in ZnO:Mn ceramics with and without magnetic field. It is worth to point out that some discrepancy between the experimental curve 3 and fitted curve 4 in Fig. 3b at wavenumbers below 400 cm^{-1} can arise from the contribution of the A_1 phonon mode, which becomes weakly active when the electric field component of the

incident radiation has a finite projection along the *c*-axis. Although the polycrystalline ZnO-based ceramics are predominantly characterized by random grain orientation as mentioned above, small fractions of grains with partial alignment of their *c*-axes to the surface normal may still contribute to the $||c$ response. This effect becomes noticeable in the low-wavenumber range, where the A_1(TO) mode is located (380–400 cm^{-1}), and leads to a slight deviation between the experimental and simulated spectra based only on the $\perp c$ configuration. Similar behavior has been previously reported for ZnO ceramics in Ref. [25].

As it was mentioned above, for undoped ZnO ceramics, the free carrier concertation was $n_0 = 7.2{\cdot}10^{17}$ cm^{-3}. Recently, it was shown that the doping with manganese resulted in the increase of ZnO:Mn grain conductivity [24]. This fact was explained by the formation of additional Zn interstitials caused by the Mn incorporation in cation lattice sites. For the ZnO:Mn ceramics studied here, the similar phenomenon occurs. The estimation of the carrier concentration shows that $n_0 = 8.0{\cdot}10^{17}$ cm^{-3} for $n_{Mn} = 10^{20}$ cm^{-3} demonstrating its increase up to $n_0 = 1.4{\cdot}10^{18}$ cm^{-3} for $n_{Mn} = 10^{21}$ cm^{-3}.

Comparing of the results obtained for ZnO and ZnO:Mn ceramics, one can conclude that magnetic field affects the specular IRR spectra via the γ_f decrease and the γ_p increase as well as slight decrease of the high-frequency dielectric permittivity. This latter was explained by the interaction of magnetic field with plasmon subsystem [5].

The application of an external magnetic field influences the damping of both phonons and plasmons primarily by modifying the dynamics of free carriers and their interaction with the lattice. The magnetic field alters carrier trajectories via the Lorentz force, affecting scattering rates and cyclotron resonance conditions, which in turn change plasmon damping parameters such as linewidth and frequency. Phonon damping is indirectly affected through modified electron–phonon coupling and changes in carrier screening, as well as possible spin-phonon interactions under magnetic fields. These effects reflect a complex interplay between charge carrier scattering, lattice vibrations, and magnetotransport phenomena. Importantly, our observations demonstrate that the magnetic field–induced changes in damping are reversible and reproducible across multiple field cycles, indicating that they arise from intrinsic, non-destructive modifications of carrier and lattice dynamics rather than permanent sample alterations.

Thus, to understand the influence of magnetic field on the infrared reflection spectra of ZnO and ZnO:Mn ceramics, it is necessary to consider its interaction with both plasmonic and phononic subsystems. One can assume that any doping favoring the formation of Zn interstitials can cause similar results.

3.2 ATR spectra of ZnO-based ceramics

Figure 4 shows the experimental ATR spectrum (symbols 1) for the ZnO ceramics with electron concentration $n_0 = 1.15{\cdot}10^{15}$ cm^{-3}. To simulate the ATR spectra, the parameters of the phonon and plasmon subsystems were extracted from the specular IRR spectra (Fig. 3b) as described elsewhere [9, 13, 17, 23]. The results are presented in Fig. 4 by the curves 2, 3, and 4 versus magnetic field strength: $H = 0$ kOe (curve 2), 65 kOe (curve 3), and 100 kOe (curve 4). The minima of the experimental and calculated ATR spectra correspond to the frequencies $\nu_{min} = 512$ cm^{-1} (1,2), 513 cm^{-1} (3), and 514 cm^{-1} (4), showing very slight shift to high-frequency range with magnetic field rise. To present curves 3 and 4 in Fig. 4 clearly, they were vertically shifted by 5% relative to curve 2. The full

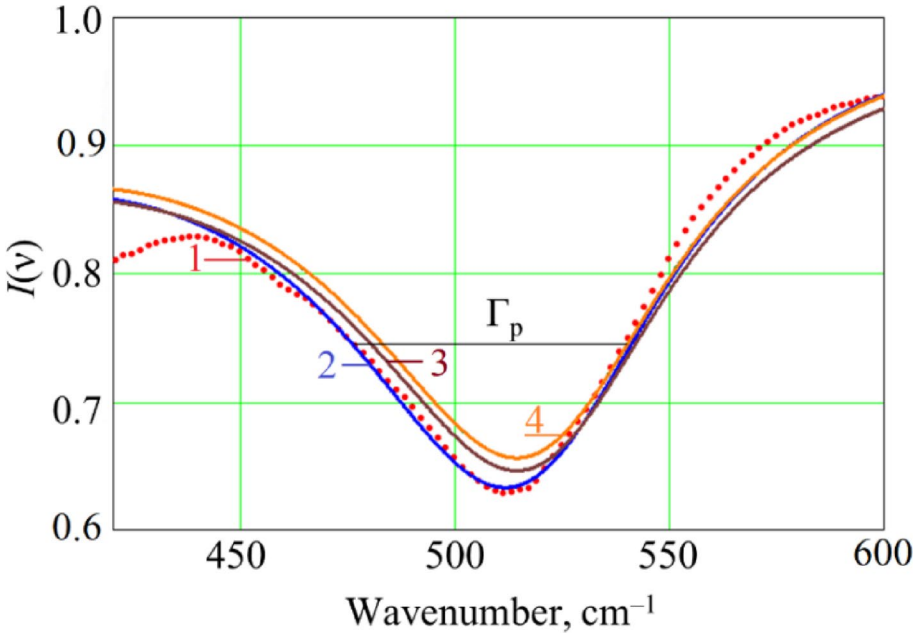

Fig. 4 Experimental (symbols 1) and theoretical ATR spectra (curves 2–4) of ZnO ceramics with carrier concentration $n_0 = 1.15{\cdot}10$ cm^{-3} versus magnetic field: 1, 2 – $H = 0$ kOe; 3 – $H = 65$ кOe; 4 – $H = 100$ кOe. $\varphi = 45°$. For the curve 2, $\Gamma_p = 29$ cm^{-1}; $\nu_{min} = 513$ cm^{-1}.

width at half maximum of the curve 2 is $\Gamma_p = 29$ cm^{-1} being similar for curves 3 and 4 (not shown). Thus, within the experimental accuracy, the effect of magnetic field on the magnitude of the ATR minimum and its spectral position is negligible for ZnO ceramics with low carrier concentration ($n_0 = 1.15{\cdot}10^{15}$ cm^{-3}).

The results for ZnO ceramics with higher concentration of free electrons ($n_0 = 1.2{\cdot}10^{18}$ cm^{-3}) are collected in Fig. 5. The experimental ATR spectrum (symbols 1) was simulated using data for plasmon subsystem $\nu_p = 325$ cm^{-1} and $\gamma_p = 400$ cm^{-1} and the values of the magnetic field $H = 0$ kOe (symbols 1 and curve 2), 30 kOe (curve 3), 65 кOe (curve 4), and 100 кOe (curve 5). As one can see, the increase of the concentration of free charge carriers up to $n_0 = 1.2{\cdot}10^{18}$ cm^{-3}, keeping constant other parameters, results in the shift of the SP frequency towards the high-frequency spectral range. Indeed, the spectral positions of the ATR minima correspond to the frequencies $\nu_{min} = 535.0$ cm^{-1} (1, 2), 534.4 cm^{-1} (3), 532.3 cm^{-1} (4), and 531.4 cm^{-1} (5), and their full width are $\Gamma_p = 88.0$ cm^{-1} (1, 2), 89.4 cm^{-1} (3), 92.3 cm^{-1} (4) and 94.2 cm^{-1} (5). The comparison of the simulating curves 2–5 (Fig. 5) reveals that an increase in the magnetic field strength leads to an increase in the full width of the SP band in the ZnO-based materials with high free electron concentration. This is accompanied by the increase of the SP damping coefficient Γ_{pp}. Using the approach described in Ref. [13] and a full width Γ_p of the SP band in ATR spectrum, the SP damping coefficients were found to be $\Gamma_{pp} = 45$ cm^{-1} (*1*, *2*) for experimental data, while further simulation versus magnetic field strength revealed the increase of Γ_{pp} up to 48 cm^{-1} (*3*), 51 cm^{-1} (*4*) and 54 cm^{-1} (*5*).

To support these findings, the comparison of the effect of magnetic field on the ART spectra of ZnO-based materials with different free carrier concentration was performed. Figure 6 shows experimental ATR spectra for undoped ZnO ceramics (curves 1, 1′) with $n_0 = 1.15{\cdot}10^{15}$ cm^{-3} and ZnO:Mn ones with $n_{Mn} = 10^{20}$ cm^{-3}, $n_0 = 8.0{\cdot}10^{17}$ cm^{-3} (curve 2, 2′) and $n_{Mn} = 10^{21}$ cm^{-3}, $n_0 = 1.4{\cdot}10^{18}$ cm^{-3} (curves 3, 3′). The analysis of these data

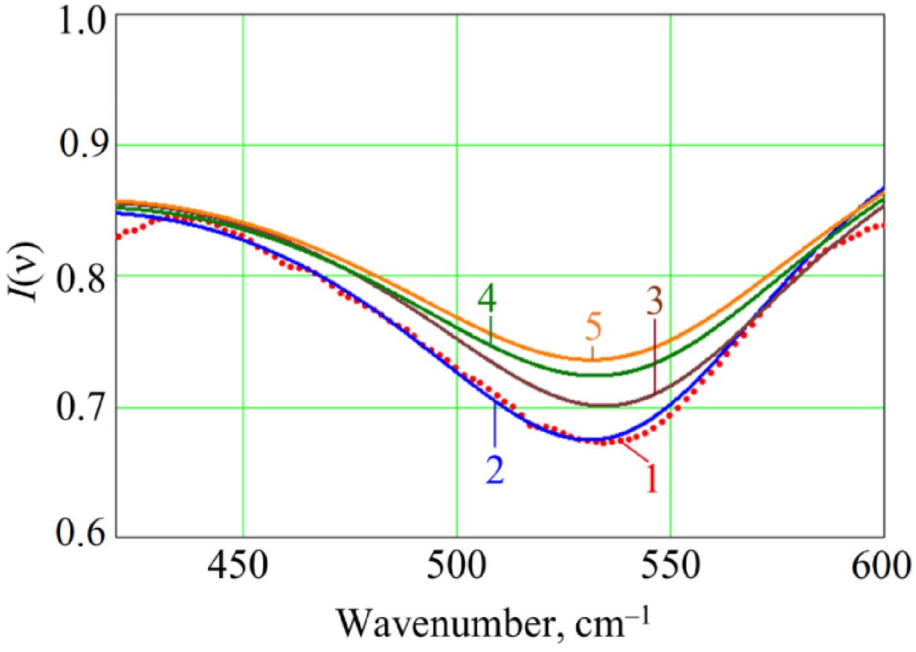

Fig. 5 Experimental (symbols 1) and theoretical ATR spectra (curves 2–4) of ZnO ceramics with carrier concentration $n_0 = 1.2 \cdot 10^{18}$ cm^{-3} versus magnetic field: 1, 2 – $H = 0$ kOe (without magnetic field application); *3* – $H = 30$ kOe; *4* – $H = 65$ kOe, *5* – $H = 100$ kOe. $\varphi = 45°$.

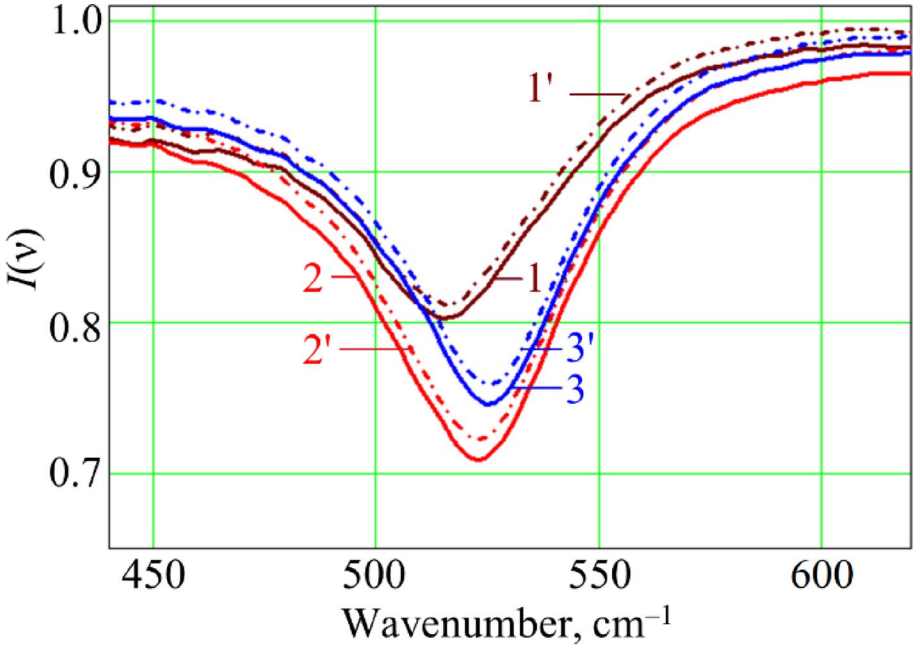

Fig. 6 Experimental (1–3) and theoretical (1′-3′) ATR spectra of ZnO ceramics with $n_0 = 1.15 \cdot 10^{15}$ cm^{-3} (1, 1′) and ZnO:Mn ceramics with $n_{Mn} = 10^{20}$ cm^{-3} (2, 2′) and $n_{Mn} = 10^{21}$ cm^{-3} (3, 3′) without (1–3) and with magnetic field $H = 10$ кОе (1′-3′). The estimated carrier concentrations are $n_0 = 8.0 \cdot 10^{17}$ cm^{-3} (2, 2′) and $1.4 \cdot 10^{18}$ cm^{-3} (3, 3′)

testifies to the spectral shift of ATR minimum due to the increase of free carrier concentration modulated by the Mn content. Indeed, the spectral positions of the ATR minima are $\nu_{min} = 515$ cm^{-1} (1, 1′), $\nu_{min} = 523$ cm^{-1} (2, 2′) and $\nu_{min} = 525$ cm^{-1} (3, 3′). The highest magnetic field of 10 kOe used in the present work did not affect significantly the

frequency of the ATR minima (Fig. 6). The full-width and damping coefficient of the SP band vary within 1%. At the same time, for this value of magnetic field, the effect of free carrier concentration in the samples is significant. Additionally, as it was discussed above, an increase in the Mn content also results in the rise of free electron concentration due to the formation of Mn_{Zn}^{2+} defects. As consequence, additional Zn interstitials donate electrons increasing their concentration and favoring the shift of the ATR minimum to the high-frequency region.

3.3 Analysis of magneto-reflectance effects in ZnO and ZnO:Mn ceramics

The parameters of the magneto-reflectance effect can be determined from the ATR spectra as proposed in [14, 20]:

$$\Delta I/I_0 = (I_0 - I_H)/I_0, \tag{3}$$

Where I_H, I_0—the amplitude of the ATR signal with applied magnetic field and without it, respectively.

Figure 7a presents the experimental dependencies of $\Delta I / I_0$ for ZnO:Mn ceramics with $n_{Mn} = 10^{20}$ cm^{-3} (curve 1) and $n_{Mn} = 10^{21}$ cm^{-3} (curve 2) under application of magnetic field with $H = 10$ кOe. The effect of magnetic field for ZnO:Mn ceramics with $n_{Mn} = 10^{20}$ cm^{-3} is observed in the range of 400–600 cm^{-1} and, in less amount, 700–800 cm^{-1} (curve 1). At the same time, for higher Mn content ($n_{Mn} = 10^{21}$ cm^{-3}), this effect is significant over whole spectral range (from 400 up to 1000 cm^{-1}) (Fig. 7a, curve 2). The effect of free carrier concentration via contribution of plasmon subsystem arises via increase of the $\Delta I / I_0$ ratio towards 1000 cm^{-1}. This result is also supported by the measurement of specular IRR spectra of the same samples in magnetic field and the estimation of the $\Delta R(\nu) / R_0(\nu)$ variation (Fig. 7b). It is seen that the effect of magnetic field on the shape of the $\Delta R(\nu) / R_0(\nu)$ dependences is more significant.

Thus, the comparison of the magneto-reflectance spectra obtained from ATR spectra (Fig. 6) and specular IR reflection spectra (Fig. 7b) for ZnO:Mn ceramics permits to assume that specular IR reflection spectroscopy is a more sensitive approach for investigation of the influence of a weak magnetic field (H ≤ 10 kOe) on optical properties of ZnO based ceramics.

Figure 8 shows the experimental frequency values extracted from corresponding ATR spectra (symbols A and B) as well as calculated dispersion curves of ZnO ceramics with $n_0 = 1.15 \cdot 10^{15}$ cm^{-3} (1,1′), $5 \cdot 10^{17}$ cm^{-3} (2, 2′) and $1.2 \cdot 10^{18}$ cm^{-3} (3, 3′) without application of magnetic field. The calculation was performed using the formulas from [5, 7] along with the data obtained from specular IRR spectra whereas phonon and plasmon damping contribution was not considered here. The calculated curves *1–3* correspond to the high-frequency dispersion branches with cut-off frequencies $\nu_s^+(k) = 541.6$ cm^{-1} (1), 553.3 cm^{-1} (2), and 575.1 cm^{-1} (3), whereas the calculated curves 1′–3′ showed low-frequency dispersion branches with cut-off frequencies $\nu_s^-(k) = 65.2$ cm^{-1} (1′), 134.0 cm^{-1} (2′), and 196.3 cm^{-1} (3′).

These results demonstrate that an increase in free carrier concentration in ZnO is accompanied by a shift of the SP frequency toward the high-frequency range. The high-frequency branches of surface polaritons, regardless of the carrier concentration in the ZnO, start at a frequency corresponding to the frequency of TO phonon $\nu = \nu_{T\perp}$, and exist at $k >> \omega/c$ ($\omega = 2\pi\nu$), asymptotically approaching the cut-off SP frequency [7,

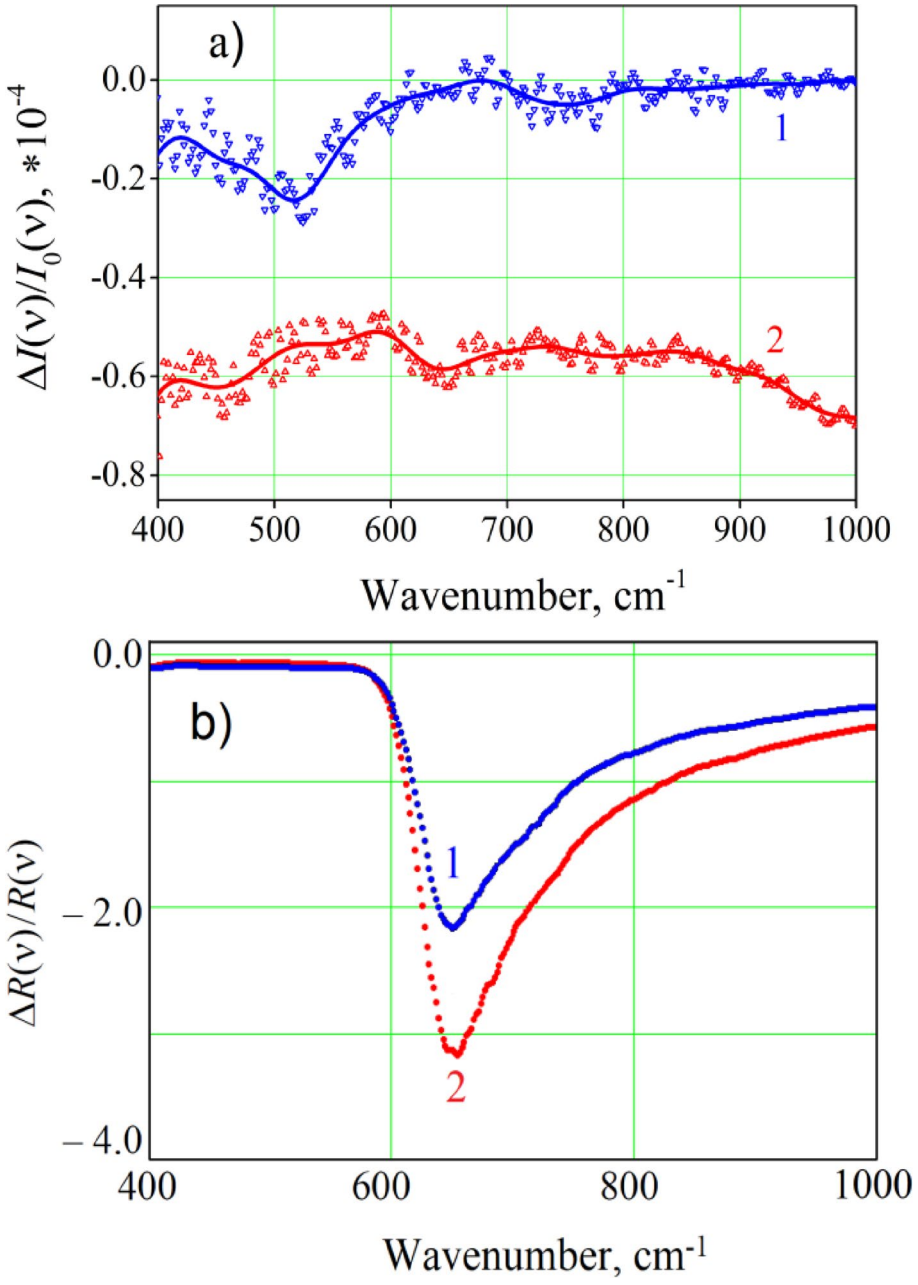

Fig. 7 Experimental dependences $\Delta I(\nu)/I_0(\nu)$ obtained from the ATR spectra (**a**) and $\Delta R(\nu)/R(\nu)$ extracted from specular IRR spectra (**b**) for ZnO:Mn ceramics with $n_{Mn} = 10^{20}$ cm^{-3}, $n_0 = 8.0 \cdot 10^{17}$ cm^{-3} (curves 1) and $n_{Mn} = 10^{21}$ cm^{-3}, $n_0 = 1.2 \cdot 10^{18}$ cm^{-3} (curves 2). $H = 10$ кОе

13]. The lack of experimental data for the low-frequency dispersion branches (below 240 cm^{-1}) is caused by the limited spectral range of our FTIR spectrometer.

The dispersion curves for ZnO ceramics with higher carrier concentration ($n_0 = 1.2 \cdot 10^{18}$ cm^{-3}) were simulated also without taking into account the phonon and plasmon damping coefficients. The effect of magnetic field strength is present in Fig. 9 for $H = 0$ kOe (curves 1, 1′), 30 kOe (curve 2, 2′), and 65 kOe (curves 3, 3′). It is seen that the high-frequency dispersion curve remains unchanged with the increase of the magnetic field strength. In contrast, the calculations showed that low-frequency dispersion branch shifts toward lower frequencies with magnetic field increasing. The curves 1′, 2′

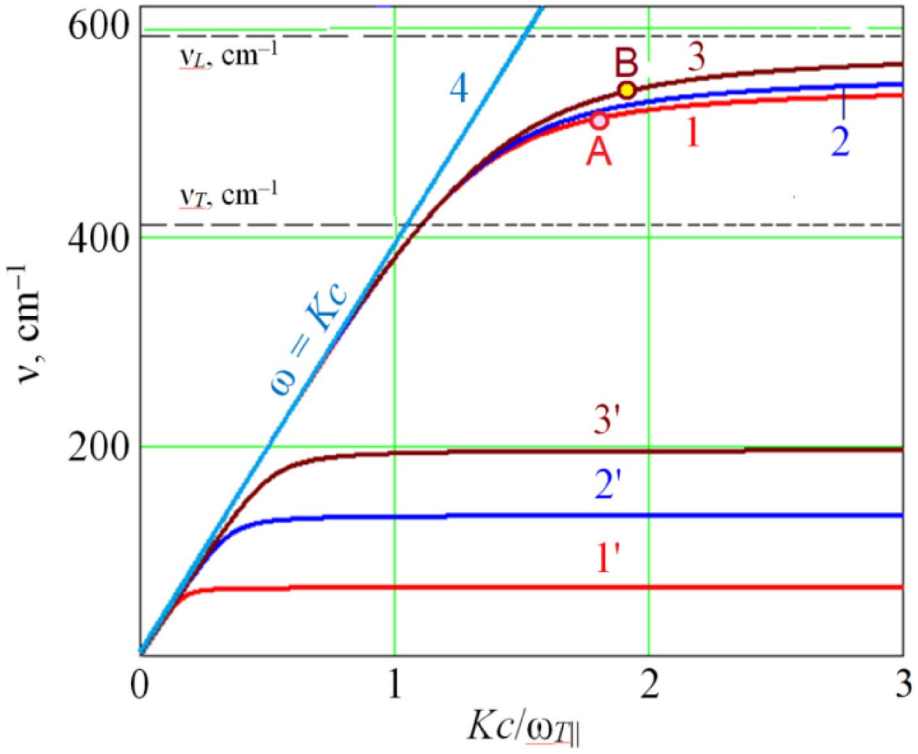

Fig. 8 High-frequency (*1*–*3*) and low-frequency (*1′*–*3′*) dispersion curves for ZnO ceramics with different free electron concentrations: 1, 1′ –n_0 = 1,15·10^{15} cm^{-3}; 2, 2′ –n_0 = 5·10^{17} cm^{-3}; 3, 3′ –n_0 = 1,2·10^{18} cm^{-3}. Curve 4 shows the light line. The symbols A and B indicate the experimental frequency values extracted from corresponding ATR spectra

and 3′ correspond to low-frequency dispersion branches with cut-off frequency values of $\nu_s^-(k)$ = 196.0 cm^{-1} (*1′*), 173.7 cm^{-1} (2′), and 147.5 cm^{-1} (3′). Furthermore, as shown in Fig. 9, the effect of magnetic field lies in the appearance of an additional dispersion branch in the 230–270 cm^{-1} spectral range (curves 4′ and 5′). When magnetic field rises from 30 kOe (curve 2′) to 65 kOe (curve 3′), the dispersion branch shifts to higher frequencies, from 200 to 300 cm^{-1}, that is caused by the increase of the cyclotron frequency Ω. The cut-off frequencies of the "pure" phonon dispersion branches are located near 232 cm^{-1} (Fig. 9, curve 4′) and 271 cm^{-1} (curve 5′). Similar effect was reported for ZnO single crystals in [13, 14, 23].

As it was mentioned above, the dispersion curves in Fig. 9 were calculated without taking into account the phonon and plasmon damping coefficients. However, when phonon and plasmon damping is considered, the variation in the reflection spectra occurs in the 390–600 cm^{-1} spectral range. For instance, for the ceramics with n_0 = 1.2·10^{18} cm^{-3}, the increase of the γ_f value from 11 to 30 cm^{-1} causes the rise of the reflectance coefficient from 0.29 to 0.36 in the 250–380 cm^{-1} frequency range as well as its decrease from 0.92 down to 0.87 in the 400–570 cm^{-1} frequency range. Similar effect was reported earlier for ZnO single crystals [14, 23].

It is worth noting that applying a strong magnetic field to ZnO crystals (see Supplementary Information, Fig. S1) promotes the appearance of a low-frequency reflection minimum in the 100–380 cm^{-1} range. The spectral position of this minimum is highly sensitive to the magnetic field strength, exhibiting a noticeable shift to higher frequencies as the field increases. These far-infrared minima reflect changes in carrier dynamics

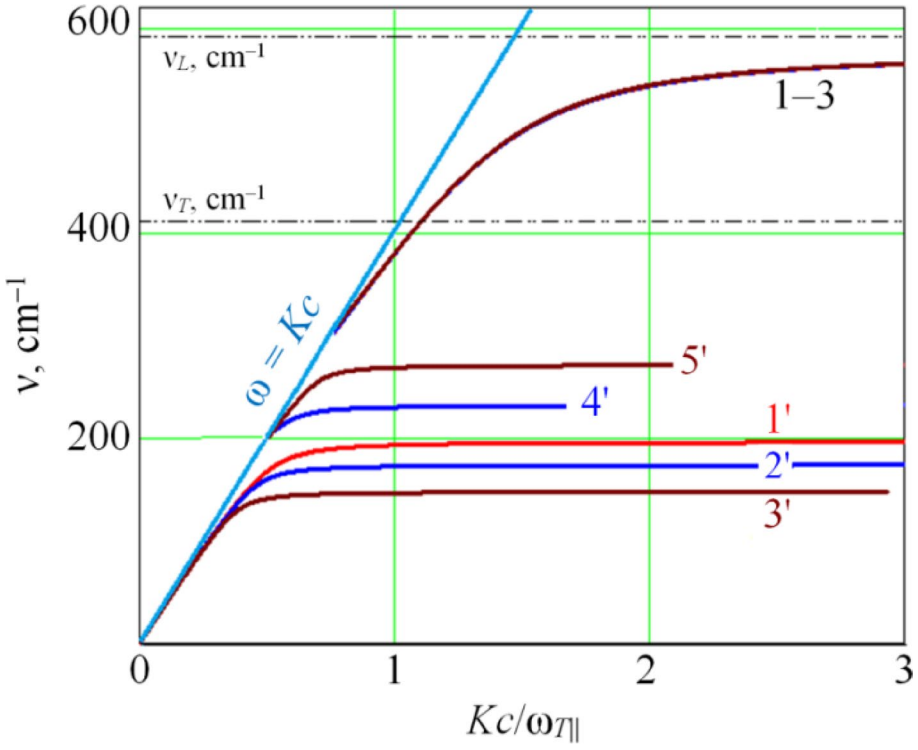

Fig. 9 Dispersion curves for ZnO ceramics ($n_0 = 1.2 \cdot 10^{18}$ cm^{-3}) under magnetic field: $H = 0$ kOe (1, 1′), 30 kOe (2, 2′,4′), and 65 kOe (3, 3′, 5′)

and spin interactions induced by the magnetic field, which can be exploited for the development of advanced sensor technologies. Sensors based on this effect are expected to demonstrate moderate to high sensitivity and ultrafast, non-contact optical response. However, their performance may exhibit notable temperature dependence, particularly when the features arise from scattering or spin-related mechanisms.

Among hexagonal semiconductors, both ZnO and GaN are viable candidates. Compared to ZnO- or GaN-based magneto-optical or plasmonic sensors, the present approach allows for non-invasive probing of ceramics and polycrystalline materials without requiring transparent substrates or polarization optics. While GaN provides excellent thermal stability and integration with electronic platforms, ZnO offers low-cost processing and greater flexibility in magnetic doping. The main limitations of the proposed method lie in its sensitivity to surface roughness and the potential need for cryogenic temperatures or high magnetic fields. Nevertheless, it represents a promising alternative for bulk magnetic sensing in complex oxide systems. Our results further suggest that such high sensitivity can also be achieved in polycrystalline ZnO ceramics and films, which is the subject of ongoing investigation aimed at advancing ZnO-based magnetic sensor technologies.

4 Conclusions

Investigating the behavior of surface phonon and phonon-plasmon polaritons in ZnO-based materials is crucial for the development of optoelectronic devices and sensors, where controlling the light-matter interaction is vital. The ability to modify the dispersion and damping characteristics of these polaritons through ZnO doping and magnetic fields renders these materials highly versatile for various technological applications. In

addition, the development of non-destructive and contactless approaches for determining materials parameters is highly required.

In this work, we demonstrated the application of infrared reflection spectroscopy for studying vibrational and carrier-related excitations in undoped and Mn-doped ZnO ceramics. Both theoretical modeling and experimental measurements were employed. For dispersion analysis, a single-oscillator dielectric model was used, incorporating additive contributions from the phonon and plasmon subsystems of ZnO. It was shown that self-consistent parameters derived from single ZnO crystals can be successfully used to predict, in the first approximation, the infrared response of polycrystalline ZnO ceramics.

Experimental and simulated spectra of specular infrared reflection and attenuated total reflection were analyzed for specific orientations of the optical axis and propagation direction of the incident electromagnetic wave. This approach allowed us to determine the phonon and plasmon parameters and to estimate the free carrier concentration within the grains. This is particularly significant for ZnO:Mn ceramics, where conventional electrical measurements are hindered by grain boundary effects. Our results indicate that Mn doping increases carrier concentration, which we attribute to the formation of Zn interstitials via Mn^{2+} substitution at cationic lattice sites.

The influence of an external magnetic field on the infrared spectra of ZnO and ZnO:Mn ceramics was also studied. Magnetic field effects were observed through variations in plasmon frequency and in the damping coefficients of both phonons and plasmons, indicating magnetically induced modifications of carrier dynamics. In the low-frequency spectral range (below the TO phonon frequency), a distinct reflectance minimum appeared, whose spectral position was found to be highly sensitive to the magnetic field strength. Although this behavior may be qualitatively consistent with polariton-related effects, we refrain from a definitive attribution to the direct propagation of surface phonon or phonon–plasmon polaritons. Nevertheless, our results highlight the potential of infrared spectroscopy as a non-destructive and contactless technique for determining the optical and electro-physical parameters of not only single crystals but also polycrystalline ZnO-based ceramics. Furthermore, the observed magnetic-field-dependent spectral changes point toward possible applications of these materials in magnetic field sensing.

Supplementary Information

The online version contains supplementary material available at https://doi.org/10.1007/s42452-025-07820-6.

Supplementary Material 1.

Acknowledgements

This work was partly supported by National Academy of Sciences of Ukraine (project III-5-21) and Ministry of Education and Science of Ukraine, as well as by the National Research Foundation of Ukraine from the state budget, project 2020.02/0380 "Structure transformation and nonequilibrium electron processes in wide bandgap metal oxides and their solid solutions".

Author contributions

O.M.: Conceptualization, Investigation, Formal analysis, Software, Visualization, Writing—original draft, Writing—review and editing. N.K.: Validation, Writing—original draft, Writing—review and editing. L.M.: Investigation, Formal analysis, Visualization, Validation, Writing—review and editing. L.K.: Validation; Resources; Investigation, Visualization, Writing—review and editing.

Funding

This work was partly supported by National Academy of Sciences of Ukraine (project III-5-21) and Ministry of Education and Science of Ukraine, as well as by the National Research Foundation of Ukraine from the state budget, project

2020.02/0380 "Structure transformation and nonequilibrium electron processes in wide bandgap metal oxides and their solid solutions".

Data availability
All data generated or analyzed during this study are included in this manuscript and its supplementary information.

Declarations

Ethics approval and consent to participate
Not applicable, as this research does not involve human participants or animals.

Consent to publication
Not applicable, as this research does not involve human participants or their data.

Competing interests
The authors declare no competing interests.

Received: 31 March 2025 / Accepted: 24 September 2025
Published online: 10 October 2025

References

1. Brion JJ, Wallis RF, Hartstein A, Burstein E. Theory of surface magnetoplasmons in semiconductors. Phys Rev Lett. 1972;28(22):1455–8. https://doi.org/10.1103/physrevlett.28.1455.
2. Brion J, Wallis R, Hartstein A, Burstein E. Interaction of surface magnetoplasmons and surface optical phonons in polar semiconductors. Surf Sci. 1973;34(1):73–80. https://doi.org/10.1016/0039-6028(73)90188-x.
3. Dmitruk NL, Litovchenko VG, Strizhevsky VL. Surface polaritons in semiconductors and dielectrics. Kyiv (Ukraine): Naukova Dumka; 1989. p. 375.
4. Kushwaha MS. Plasmons and magnetoplasmons in semiconductor heterostructures. Surf Sci Rep. 2001;41(1–8):1–416. https://doi.org/10.1016/s0167-5729(00)00007-8.
5. Tarkhanyan RH, Uzunoglu NK. Radiowaves and Polaritons in Anisotropic Media: Uniaxial Semiconductors. KGaA, Weinheim: Wiley-VCH Verlag GmbH & Co; 2006.
6. Venger EF, Evtushenko AI, Melnichuk LY, Melnichuk AV. Reflectance spectra of a 6H-SiC single crystal placed in a strong homogeneous magnetic field. J Eng Phys Thermophys. 2009;82(6):1211–8. https://doi.org/10.1007/s10891-010-0297-3.
7. Sloan J, Rivera N, Joannopoulos JD, Kaminer I, Soljačić M. Controlling spins with surface magnon polaritons. Phys Rev B. 2019;100(23):235453. https://doi.org/10.1103/physrevb.100.235453.
8. Autore M, D'Apuzzo F, Di Gaspare A, Giliberti V, Limaj O, Roy P, et al. Plasmon-phonon interactions in topological insulator microrings. Adv Opt Mater. 2015;3(9):1257–63. https://doi.org/10.1002/adom.201400513.
9. Melnichuk O, Melnichuk L, Venger Y, Guillaume C, Chauvat M, Portier X, et al. Optical, structural and electrical characterization of pure ZnO films grown on p-type Si substrates by radiofrequency magnetron sputtering in different atmospheres. Semicond Sci Technol. 2020;35(9):095034. https://doi.org/10.1088/1361-6641/ab9397.
10. Bhuyan R, Mony J, Kotov O, Castellanos GW, Rivas JG, Shegai TO, et al. The rise and current status of polaritonic photochemistry and photophysics. Chem Rev. 2023;123(18):10877–919. https://doi.org/10.1021/acs.chemrev.2c00895.
11. Chochol J, Postava K, Čada M, Pištora J. Experimental demonstration of magnetoplasmon polariton at InSb(InAs)/dielectric interface for terahertz sensor application. Sci Rep. 2017. https://doi.org/10.1038/s41598-017-13394-0.
12. Palik ED, Kaplan R, Gammon RW, Kaplan H, Wallis RF, Quinn JJ. Coupled surface magnetoplasmon-optic-phonon polariton modes on InSb. Phys Rev B, Solid State. 1976;13(6):2497–506. https://doi.org/10.1103/physrevb.13.2497.
13. Venger IV, Venger EF, Melnichuk LYu, Melnichuk OV. Anisotropy of surface plasmon-phonon polaritons in ZnO and 6H-SiC, Naukova dumka, Kyiv (Ukraine); 2020. p.192. ISBN 978-966-00-1792-4 (in Ukrainian).
14. Melnichuk OV, Korsunska NO, Melnichuk LYu, Markevich IV, Borkovska LV, Khomenkova LYu, Venger EF. Structural transformation and non-equilibrium electron processes in wide bandgap oxides and their solid solutions, Mykola Gogol Nizhyn State University, Nizhyn (Ukraine); 2024. p. 274. ISBN 978–617–527–301–2 (in Ukrainian).
15. Oliveira F. Faraday Effect and other Magneto-Optic Effects in Semiconductors, PhD thesis, University of Minho, Braga, Portugal; 2015. https://doi.org/10.13140/rg.2.1.1319.6881.
16. Lan T, Ding B, Liu B. Magneto-optic effect of two-dimensional materials and related applications. Nano Select. 2020;1(3):298–310. https://doi.org/10.1002/nano.202000032.
17. Melnichuk O, Korsunska N, Markevich I, Boyko V, Polishchuk Y, Tsybrii Z, et al. Peculiarities of specular infrared reflection spectra of ZnO-based ceramics. Semicond Phys Quantum Electron Optoelectron. 2021;24(04):390–8. https://doi.org/10.15407/spqeo24.04.390.
18. Forecast R, Gholizadeh EM, Prasad SKK, Blacket S, Tapping PC, McCamey DR, et al. Power dependence of the magnetic field effect on triplet fusion: a quantitative model. J Phys Chem Lett. 2023;14(20):4742–7. https://doi.org/10.1021/acs.jpclett.3c00919.
19. Hayashi H, Sakaguchi Y, Abe H. Magnetic field effects on dynammic behavior of excited molecules. Physica B. 1990;164(1–2):217–21. https://doi.org/10.1016/0921-4526(90)90079-a.
20. Kravets VG, Poperenko LV, Yurgelevych IV, Pogorily AM, Kravets AF. Optical and magneto-optical properties and magnetorefractive effect in metal-insulator CoFe–Al_2O_3 granular films. J Appl Phys. 2005. https://doi.org/10.1063/1.2009814.
21. Venger EF, Ievtushenko AI, Melnichuk LYu, Melnichuk OV. Investigation of ZnO single crystals subjected to a high uniform magnetic field in the IR spectral range. Semicond Phys, Quantum Electron Optoelectron. 2008;11(1):6–10. https://doi.org/10.15407/spqeo11.01.006.
22. Venger EF, Ievtushenko AI, Melnichuk LYu, Melnichuk OV. Effect of strong magnetic field on surface polaritons in ZnO. Semicond Phys, Quantum Electron Optoelectron. 2010;13(3):314–9. https://doi.org/10.15407/spqeo13.03.314.

23. Melnichuk O, Melnichuk L, Venger E. Phonon and Plasmon-Phonon interactions in ZnO single crystals and thin films, chapter 7 in O*xide-based materials and structures: Fundamentals and Applications*. In: Savkina R, Khomenkova L, editors. Boca Raton: CRC Press; 2020. pp.163–199
24. Korsunska N, Markevich I, Stara T, Polishchuk Yu, Ponomaryov S, Kozoriz K, et al. Influence of compacting pressure on the electrical properties of ZnO and ZnO:Mn ceramics. Discov Appl Sci. 2024;6(3):74. https://doi.org/10.1007/s42452-024-05722-7
25. Melnichuk OV, Korsunska NO, Markevich IV, Boyko VV, Polishchuk YO, Tsybrii ZF, et al. Peculiarities of specular infrared reflection spectra of ZnO-based ceramics. Semicond Phys, Quantum Electron Optoelectron. 2021;24(4):390–8. https://doi.org/10.15407/spqeo24.04.390.

Publisher's Note